Automated UAV Controller Synthesis via LLM-Generated Control Logic and Particle Swarm Optimisation

***Abstract*—LLM-guided evolutionary frameworks for program synthesis have demonstrated strong results across combinatorial benchmarks; however, such frameworks have not been widely explored for robotic control systems. This paper presents an automated framework for synthesising control logic and optimising numerical coefficients, enabling the deployment of generated controllers onto robotic platforms. To produce deployable controllers, the framework separates control logic synthesis from numerical parameter optimisation, with controller coefficients optimised via Particle Swarm Optimisation using a Markov Decision Process reward signal. The resulting controllers are evaluated in a custom UAV simulation environment, validated using PX4 Software-In-The-Loop, and subsequently deployed on a physical UAV. Controller performance is evaluated on Lemniscate and Lissajous trajectory-tracking tasks and compared against PID with disturbance observer and Linear Quadratic Regulator baselines. Across both trajectories, the framework-generated control law achieves improved tracking accuracy relative to the baseline controllers, with a minimum reduction in mean squared error of approximately 38% in real-world experiments. These results demonstrate the feasibility of deploying automatically synthesised control logic on a physical UAV, bridging automated program synthesis and real-world control deployment.**

Large Language Models, Optimisation, Control, Unmanned Aerial Vehicles

I. Introduction

DESIGN and testing of high-performance control systems for Unmanned Aerial Vehicles (UAVs) is a difficult and time-consuming process that relies on expert knowledge. ~~While classical~~ Within UAVs, control systems such as Proportional-Integral-Derivative (PID) and Linear Quadratic Regulator (LQR) remain widely used~~, their~~. Unfortunately, PID and LQR performance is sensitive to modelling inaccuracies, parameter selection, and operating conditions. More recently, ~~reinforcement learning~~ Reinforcement Learning (RL) methods have shown promise in ~~automating controller design~~ UAV controller design [**?**]; however, their reliance on training data and the sim-to-real gap continue to limit their widespread adoption~~in real-world systems~~.

In parallel, Large Language Models (LLMs) have emerged as powerful tools used for much more than ~~simple question and answer~~ chatbots [**?**]. LLMs are now being utilised for program synthesis and optimisation across a wide range of domains [**?**]. Recent work has demonstrated that LLMs can generate functional code, assist local search, and even outperform human-designed heuristics in combinatorial tasks [**?**]. Despite this progress, the application of LLMs to UAV control system synthesis remains unexplored, with little evidence that LLM-generated algorithms can be deployed on physical systems. Key challenges include the appropriate selection of program parameters, evaluation of control systems under model mismatch, and the transition from simulation to real-world execution.

This work addresses these challenges by proposing ~~an automated~~ a framework that combines LLM-based program synthesis with classical optimisation and real-world ~~validation~~deployment. Rather than relying on LLMs to optimise ~~continous~~ continuos parameters directly, we deliberately decouple controller structure from parameter tuning. In ~~the proposed~~ our approach, LLMs ~~are responsible for generating control logic, while real-valued coefficients are optimised using~~ propose a control system for a UAV and any coefficients within that program are optimised via Particle Swarm Optimisation (PSO). This separation of responsibilities closely aligns with established practises within Symbolic Regression (SR) and evolutionary control ~~, enabling each component to operate within its own~~- using each component for its own' strengths.

Controller designs are refined through a multi-shot evolutionary querying strategy. Previous controller programs and their performance metrics are incorporated into subsequent LLM queries, enabling ~~a guided~~ an optimisation procedure with quantitive feedback. An actor-critic LLM loop is employed, whereby one model proposes control logic and another provides recommendations based on results.

The proposed framework is evaluated on a thrust-and-torque ~~quadcopter~~ UAV control problem. Controllers are trained in a custom UAV environment, validated in PX4 SITL, and finally deployed onto a real UAV. Performance is assessed on two ~~challenging~~ trajectory-tracking tasks and compared against a PID+DOB and LQR controller. The results demonstrate that the LLM-generated control system achieves superior tracking and robustness across simulated and real-world ~~and simulated~~ experiments.

The primary contribution of our paper is the deployment of ~~a generated~~ an LLM-generated control system to a UAV. Our results position LLM-assisted controller design as a viable and scalable tool for engineering applications, bridging the gap between ~~automated~~ UAV controller design and real-world deployment.

II. Related ~~Papers~~Works

The problem this work focuses on solving is the deployment of generated algorithms in ~~the real world~~to a robotic control system. The current technical issues faced when trying to implement such a solution are related to the choice of the parameters for a given computer program, and scoring the quality of the produced computer programs within the simulation due to model mismatch. Our specific contributions, to

that end, are: multi-shot local policy search, training and test environments, and a method that utilises a UAV platform to test generated control algorithms.

In the literature, the most related paper to our work appears to be 'LLM-Assisted Local Search for Policy Synthesis' [?] . With Sadamine, Baier, and Lelis's work, they demonstrate how LLMs can be used to create programmatic Using LLM-assisted local search for policy synthesis, it is possible to create programmtic policies for various tasks within a single shot. Notably, our work differs from theirs in two separate instances: our policies are tested in these works are not tested within the real world, and we focus on multiple queries to the LLM for program synthesis. Based on our previous work, it appears that a wide approach to program synthesis has provided better results than a small initial population for performing the local search .

In terms of evolutionary papers related to ours, the basis for this paper is FunSearch [?]. Within FunSearch, the authors demonstrated how evolutionary queries can be utilised to only contain singular queries [?]. FunSearch furthers LLM-assisted local search by performing GA-like operations across generated policies [?]. Using GA-like evolutionary techniques showcases how LLM-assisted evolutionary searching can produce heuristics that surpass human performanceon combinatorial problems. Compared to our work, which focuses on both evolutionary and local parameterisation, the FunSearch method is costly and yields significantly worse results. The primary reasons behind the increased cost of FunSearch are related to local parameterisation. It is unlikely that the FunSearch technique, on its own, can be used to create a high-quality control system within a reasonable time or without incurring significant excess computational cost. The inefficiencies of FunSearch are due to the choice of coefficient values within program synthesis. Opposed to simply altering a variable value, the FunSearch technique typically opts for a more complex solution to a problem. .

Li et al. [?] focused on an enumerative search technique for program synthesis. Li et al.'s work focuses primarily on the synthesis of programs for solving a complex dataset (SyGuS), with a continuous bi-directional communication feedback loop for failed programs. The primary contribution of their research is the creation Implementing an actor-critic loop within evolutionary search is shown to increase the quality of programs as solutions for complex datasets - via the usage of a 'probabilistic Context-Free Grammar(pCFG)' , a list of failed programs, to help the LLM achieve a correct solution. A similar technique is used in our methodology. Opposed to giving a specific name to this technique, we define how and why we implemented it. For our work, we instead focus on the implicit information provided to the LLM through evolutionary queries and epigenetic program selection. Our evolution queries include previous examples of programs, along with a meta-heuristic, the 'score' of a program. Theoretically, providing the programs in the query as our approach, as opposed to theirs, provides increased context for the model to make intelligent decisions. Our work, rather than focusing on achieving a broad application of the technique, aims to apply the optimisation to a single use case. This allows us to incorporate information easily and include meta-heuristic information into our queries—a difficult task to achieve in the broad sense.' [?]. It is also possible to improve the quality of critiquing within solutions by introducing multi-modality [?], however, due to cost constraints this technique is not used within our work.

A related work that might help support the theoretical results of this approach, which has not been implemented, is the usage of multimodality within query generation before program synthesis. For example, Huang et al. [?] performed work utilising GPT-4's multimodal features, demonstrating how multimodality can enhance optimisation performance. In the context of our work, implementing this makes sense simply due to the ease and clarity with which information about a trajectory can be displayed in a visual format. However, a decision was made not to incorporate multimodal queries within our results, primarily due to our incentive to keep the monetary cost of generation at zero. We believe that ensuring the optimisation process is free increases much-appreciated scrutiny and facilitates widespread adoption.

For a recent review and survey of papers covering the relevant topic area, the authors recommend either Wu et al. [?] or Huang et al. [?]. Both papers provide a comprehensive overview of the current progress in Large Language Models and Optimisation.

The reasoning behind this decision is that PSO has proven effective on a range of control problems. For example, researchers have applied PSO to automatically tune PIDgains for UAV attitude and position control , achieving improved trajectory tracking performance without manual tuning [?] . UAV control is largely dominated by four main control systems: PID [?], Reinforcement Learning [?], MPC [?], and non-predictive model-based methods [?]. PID controller remain the dominant control system, due to ease of use. The issues with PID are the requirement for tuning for optimal performance. RL is currently the optimal technique, however relies on extensive model building and environmental data. MPC has the same drawbacks as RL, however it also requires a lot of compute during runtime to compute optimal trajectories. Finally, LQR based method are focused on the drawbacks of PID, making tuning easier. The problem with LQR is the requirement for an algebraic equation to be solved for optimal control each timestep, and the expertise required to implement the model for the control system.

To our knowledge, no one has yet deployed a generated algorithm in the real world. Evolutionary robotics and GP-based techniques have been investigated for control system usage, usually parametrised via neural or symbolic structures [?]. Our work instead focuses on tractable LLM-generated control laws.

Unlike optimal control formulations that assume known model structure and quadratic costs [?], this work automates the synthesis of the control structure itself.

III. Methodology

Our approach employs a dual-query Large Language Model (LLM) framework to automatically synthesise a thrust/torque

UAV controller. A primary critic LLM first generates a high-level specification for a controller, and a secondary critic LLM analyses simulation responses and suggests feedback. Collaboration between the actor and critic forms an actor-critic LLM loop, motivated by successes in LLM-assisted program synthesis [**?**]. LLMs can produce functional code for most tasks, but pairing with a critic or verification step improves reliability ~~[?]~~ [**?**]. When implemented in this manner, the LLM is proposed to refine its output based on performance, which is synonymous with self-reflection and In-Context-Learning (ICL) ~~[?]~~ [**?**]. By incorporating a critic model, we improve performance, similar to recent LLM approaches that use an agent to verify actions ~~[?]~~ [**?**]. The two LLMs operate together: the primary LLM proposes a control logic structure, and the secondary LLM implements the logic and provides quantitative feedback.

A key and deliberate feature of our method is the abstraction of code logic and the optimisation of numerical coefficients. The LLM pair performs high-level decision making and program synthesis (e.g., controller design, conditional logic), with the real-valued coefficients (e.g., vehicle mass and controller gains) of the program optimised via classical methods. The reasoning behind this deliberate abstraction is simple: LLMs excel at writing structured code from descriptions and making high-level decisions, yet lack direct real-value optimisation capability. Our approach mirrors that of Symbolic Regression, whereby a genetic programming technique evolves a high-level topology, with classical optimisers tuning constants [**?**]. Similarly, our approach produces a human-readable control policy, with placeholder values treated as tunable parameters. This separation of responsibilities is advantageous as it combines expert knowledge ingested by LLMs during training with the search capabilities of optimisation for real-valued parameters. We refer to this separation of duties as program specification (controller design) and program parameterisation (optimisation of parameters).

To implement the program parameterisation stage, we use Particle Swarm Optimisation (PSO). In our specific case, each particle represents a set of program coefficients (e.g., PID gains). The PSO algorithm optimises the coefficients to minimise the trajectory-tracking error for a given program. The simulated fitness score enables the PSO algorithm to converge towards a suitable parameter set for each controller. We modified the standard PSO algorithm to enhance the global stability criteria for our problem.

Firstly, the inertia decays over time, resulting in exploitation of the search space nearer the end of the search [**?**]:

$$\omega(t) = \omega_{\max} - \left(\frac{\omega_{\max} - \omega_{\min}}{T}\right) t \tag{1}$$

with $\omega_{\max}$ and $\omega_{\min}$ representing the maximum and minimum inertia, ~~and~~ T representing the total number of iterations, and t representing the current timestep.

Time-varying acceleration coefficients for social and personal coefficients are also applied to the algorithm [**?**]:

$$c_1(t) = c_{1,\min} + (c_{1,\max} - c_{1,\min}) \frac{t}{T} \tag{2}$$

$$c_2(t) = c_{2,\max} - (c_{2,\max} - c_{2,\min}) \frac{t}{T} \tag{3}$$

And finally, the velocity is clamped such that particles cannot move too fast across the search space [**?**]:

$$PSv_{\max}(t) = v_{\max,\ \text{initial}} - \left(\frac{v_{\max,\ \text{initial}} - v_{\max,\ \text{final}}}{T}\right) t. \tag{4}$$

To further refine the generated solution, another local search step is performed upon the optimal program before deployment and testing. We take the best solution from PSO and perform a larger optimisation step to ensure that a better set of coefficients has not been missed. That is, a course initial optimisation is performed, followed by a finer second optimisation on the best-scoring program. The justification for this step stems from analyses of PSO, which indicate that PSO converges to local optima without guaranteeing global optimality ~~[?]~~ [**?**]. This final search exploits the best solution and fine-tunes parameters for minor performance improvements. Essentially, PSO is used in a global sense under broad search constraints, and a subsequent search is performed to refine the result. A combination of a final, deeper refinement stage with a fast-searching stage enables the finalisation of our algorithm, which identifies a near-optimal set of coefficients for the generated controller.

A. *Implementation pipeline*

Notably, all the steps listed below are automated, and our algorithm requires only a description of the problem and the loss function to begin optimisation. See Figure **??** for a general overview of this automated process.

We begin by querying the LLM with a detailed description of the task at hand and specific requirements. For our case, this prompt also included an example base controller (PID). It is not necessary to include a base template, as discussed in [**?**]; however, faster convergence is achieved with a given base. The prompt also includes structural and typographic information (C++, return values, frame translations). We also ensure that the prompt consists of details on placeholder coefficient gains and how to access them. The actor LLM's response produces an initial set of viable population members. For each response we receive, we ensure that it compiles without runtime or compilation errors before assuming it is a valid response. For any set of invalid responses received, the actor LLM is queried again for a new output until a complete set of admissible programs is available for testing.

The admissible set of responses is then integrated into the simulation environment to perform optimisation. We run our RVO stage to estimate each controller's performance. The final fitness for each computer program is recorded in a Table, along with the program's identification number (ID) and score. The loss function is designed so that the minimum score in the Table above corresponds to the identification number of the optimal-performing program. Any number of elite population members can be saved for the next generation and appended to the next generation's query. Realistically and pragmatically,

Fig. 1: **System overview:** An overview of the LLM for optimization process.

in our algorithm, it only makes sense to keep the most elite population member.

The environment and experiments are an ad-hoc UAV simulation based on Flightmare (details of which are listed in Section **??**) [**?**]. The environment allows us to place the LLM's output ‘in-testing’, enabling automated observation of behaviours with performance metrics.

The automated metrics are provided to the critic LLM, along with the code, to integrate high-level observational critiques into the actor's control design. During this stage, multimodality could be a key feature. Providing a visual demonstration of the current optimal controller output could lead to better insights into actionable goals for the actor to implement. For example, the critic that provides information such as ‘the drone overshoots the target‘ offers much better insight into the program's performance than descriptions of performance metrics. Multimodality has not been implemented in our algorithm due to both cost constraints and scope. The critic output and observations are appended to the query for the next generation of the population, thereby providing closed-loop feedback. This collaborative feedback loop creates an actor-critic dynamic and aligns with emergent LLM practices of using self-reflection to refine solutions.

Upon receiving the critic's response regarding program performance, we begin defining the query for the actor to produce the next generation. The new query starts again with the problem description and specific requirements, which we consider static and never change during program evolution. Exponentially sampled (based on score) examples of previous population members are included in the new query. The reasoning behind an exponential sample of the program history is based on our understanding of Epigenetic DNA, whereby previous genes are not forgotten; they are less likely to be expressed. After joining the previous examples onto our new query, we add the critic's response. This new query forms the basis for the actor's implementation of the next-generation population.

The process is repeated until either the convergence criteria are met or the maximum number of iterations is reached. In summary, the stages are: query construction, actor program synthesis, real-valued optimisation, population selection, and critiquing. A general overview of this process is provided for easy viewing in Figure **??**.

Our custom simulation environment is designed as a Markov Decision Process (MDP) chain, which integrates UAV dynamics. It is possible to reset the simulation, view rewards, apply control actions, and retrieve observations at each timestep. This allows for easy integration with the RVO optimisation step, in which the cumulative sum of rewards serves as the loss function for each rollout, and the simulation can be reset for each particle. The simulation operates with an 8ms interval for physics updates and control loops. By framing our simulation as an MDP, we ensure reproducibility and ease of scenario configuration. All simulations were run on a 32-core computer without using a GPU. Each simulation rollout took a few seconds, so the total optimisation and testing of the generated controls took around 5 minutes per iteration. For our full simulation, we ran for 100 generations, using a population size of 30. For the PSO parameters, we used 300 particles with 10 dimensions. For fine-tuning the final model, we used 10,000 particles across 10 dimensions. The PSO particles were had no bounds for exploration, due to the general purpose usage of the program coefficients, however, they were initialised uniformly within the range $[-1, 1]$. Particle velocity was clamped to a maximum value of 1.0, such that both large and small coefficients could be effectively explored. Dynamic social and personal weighting was in effect, discussed in Section **??**, however the initial value for the social c_1 and personal c_2 parameters was set to 0.5 and 0.8 respectively. In total, we trained for around 30 minutes before seeing results that outperformed the baseline. The full training loop (100 iterations) took 5 hours. Exact token usage was not calculated during the training process, and requires further investigation. For the full training procedure, the cost whilst using GPT 3.5-turbo came to be £0.80 (GBP).

For the LLM querying, GPT-3.5 turbo was used with a temperature setting of 0.6 and a top_p value of 0.1. The context window length of GPT 3.5-turbo, 4,096 tokens, had enough space to fit both parts of the query; the static and evolutionary query parts both fit inside the context window.

B. *The critic*

The critic performs an analysis of the provided control system and offers areas for improvement. Each generation,

the optimal program per-island is provided to the critic for analysis. The critic determines issues with the control system and provides recommendations on areas for improvement. The critic response is appended to the primary population candidate query for the next generation. This forms a closed loop, whereby current optimal programs are critiqued, improved, and critiqued again. In our research, we used the same model (GPT-3.5-turbo) for the critic as the main program.

C. Simulated training environment

The equations used to describe the UAV and its movement across time are supplied by the vast research done by [**?**], [**?**], [**?**], [**?**].

To control the UAV, we utilise mass-normalised collective thrust and body-torque ($A \in \mathbb{R}^4$) measured in Newtons. The upper bound of the collective thrust is calculated as the maximum thrust produced by all four motors, as determined by measurements. The maximum body torque is the most significant differential between any two given motors.

To simulate thrust from the given outputs, the control policy output is first converted into motor angular velocity (RPM), denoted $r_i^{des} \in \mathbb{R}^4$, the equations for which are given by

$$r^{des} = IA\omega_t' + \omega' \times (I\omega'), \tag{5}$$

with A being the motor allocation matrix, provided as

$$\mathbf{A} = \begin{bmatrix} 1 & 1 & 1 & 1 \\ l\sqrt{\frac{1}{2}} & -l\sqrt{\frac{1}{2}} & -l\sqrt{\frac{1}{2}} & l\sqrt{\frac{1}{2}} \\ -l\sqrt{\frac{1}{2}} & -l\sqrt{\frac{1}{2}} & l\sqrt{\frac{1}{2}} & l\sqrt{\frac{1}{2}} \\ k_1 & -k_2 & k_3 & -k_4 \end{bmatrix}.$$

The RPM is then passed through a first-order motor model to simulate the motor's internal dynamics,

$$\dot{r_i} = \frac{1}{\alpha_i}(r_i^{des} - r_i) \tag{7}$$

where α_i is the motor ramp time for the ith rotor.

A linear model based on data from the UAV motors is used to convert the RPM of the motor into thrust:

$$f_i = r_i^2 \cdot M_c \tag{8}$$

Where M_c is the constant for the motor-propeller pair. These thrust values allow the definition of a three-axis body torque matrix $\eta \in \mathbb{R}^3$ and collective thrust c:

$$\eta = \begin{bmatrix} \frac{l}{\sqrt{2}}(f_1 - f_2 - f_3 + f_4) \\ \frac{l}{\sqrt{2}}(-f_1 - f_2 + f_3 + f_4) \\ k_1 f_1 - k_2 f_2 + k_3 f_3 - k_4 f_4 \end{bmatrix}, \tag{9}$$

$$c = f_1 + f_2 + f_3 + f_4, \tag{10}$$

where l is the UAVs arm length, f_i is the thrust produced by the motors, and k_i is the rotor drag co-efficient.

Given the filtered body torque and collective thrust, it is possible to transition between timesteps with the following equations (note Lagrange notation for derivatives):

$$P' = V \tag{11}$$

$$V_{wb}' = Q_{wb} \odot c - G - RDR^T v \tag{12}$$

$$Q_{wb}' = \frac{1}{2}\lambda(\omega_{wb}) \cdot q_{wb} \tag{13}$$

where $\lambda(\omega_{wb})$ is a skew-symmetric matrix of the vector $(0, \omega^T)^T = (0, \omega_x, \omega_y, \omega_z)^T$.

$$\omega_{wb}' = I^{-1} \cdot (\eta - \omega_{wb} \times I\omega_{wb}) \tag{14}$$

where $G = [0, 0, -g]^T$, $R \in \mathbb{R}^{3,3}$ is a rotation matrix of the form $R = \{X_b, Y_b, Z_b\}$, D is a diagonal matrix defining rotor drag coefficients $D = diag(d_x, d_y, d_z)$, $\odot$ denotes the multiplication of a vector and quaternion, and the inertia matrix I of the UAV is given by $\mathbf{I} = \text{diag}\{I_{xx}, I_{yy}, I_{zz}\}$ in which each $I_* \in \mathbb{R}$ is the moment of inertia about each of the UAV's body-axes.

The following equation is used to estimate the UAV's inertia, which we use throughout the simulation.

$$\hat{I} = \frac{m}{12} l^2 D \tag{15}$$

For the observation state of the policy, Brownian motion noise is added to the linear and angular velocities, simulating both a random walk and a per-timestep disturbance. The noise added to the environment is somewhat complicated to write down mathematically, so ~~a GitHub link is provided for those who wish to view~~ https://github.com/PX4/PX4-SITL$_gazebo-classic/blob/70683dc759cbd3ebccfa78429b564f8b1fb5d149/src/gazeb$

Each timestep, the controllers recieves a state $S = [P, \Omega, P', \Omega'], S \in \mathbb{R}^{12}$, and provides the desired body torque and collective thrust $A = [a_0, a_1, a_2, a_3], A \in \mathbb{R}^4$.

The values we use for our UAV are provided in Table **??**

TABLE I: Quadcopter Model Parameters

Symbol	Value
g	$9.81\,\text{m/s}^2$
α^{-1}	$0.0125\,\text{s}$
Δt_{sim}	$0.008\,\text{s}$
M_c	7.84×10^{-6}
k_i	1.75×10^{-4}
m	$2.0\,\text{kg}$
l	$0.225\,\text{m}$
D	diag(4.5, 4.5, 7)

All results are provided and calculated using ~~either~~ the Mean Squared Error (MSE) ~~or Sum of Squared (SSE) errors. Thus, both SSE and MSE are given~~ of positional reference error across all axis, in m^2 units. ~~These are all calculated as the mean error across all axes.~~

D. ~~Experiments~~

~~Our custom simulation environment is designed as a Markov Decision Process (MDP) chain, which integrates UAV dynamics. It is possible to reset the simulation, view rewards, apply control actions, and retrieve observations at each timestep. This allows for easy integration with the RVO optimisation step, in which the cumulative sum of rewards serves as the loss function for each rollout, and the simulation can be reset for each particle. The simulation operates with an 8ms interval for physics updates and control loops. By~~

framing our simulation as an MDP, we ensure reproducibility and ease of scenario configuration. All simulations were run on a 32-core computer without using a GPU. Each simulation rollout took a few seconds, so the total optimisation and testing of the generated controls took around 5 minutes per iteration. For our full simulation, we ran for 100 generations, using a population size of 30. For the PSO parameters, we used 300 particles with 10 dimensions. For fine-tuning the final model, we used 10,000 particles across 10 dimensions.

D. Trajectory Tracking

The primary task for the generated controller was to accurately track an oscillating lemniscate trajectory. We chose a lemniscate as the reference position, as it is a complex trajectory to follow. The lemniscate requires the UAV to perform continuous turns in opposite directions, thereby exciting the UAV's dynamics and challenging the controller's response. We define the lemniscate trajectory as:

$$P_r^t = \begin{bmatrix} rad\,\sin\big(\theta(t)\big), \\ rad\,\sin\big(2\,\theta(t)\big), \\ z_0 + \sigma(t)\,A\,\sin\big(\theta(t)\big) \end{bmatrix} \tag{16}$$

with rad controlling the circle radius, z_0 controlling the height, t is the timestep multiplied by Δt, A controlling the vertical offset, and $\theta(t)$ provided as

$$\theta(t) = 2\pi\frac{t}{T}. \tag{17}$$

Our experiment is designed so that each rollout completes in 40 seconds, yielding 10,000 simulation timesteps. As noted in prior work, lemniscate trajectories exhibit rapid, coordinated attitude changes while maintaining stability. The initial state for the quadcopter at $t = 0$ is provided as some distance away from the trajectory's initial position: $P_x = 1$, $P_y = -1$. Additionally, the controller starts with a large yaw offset. Implementing an initial positional offset and rotational bias allows us to estimate the controller's performance for large and small reference errors within a single simulation run. Tracking performance is evaluated using a standard metric: the Sum of Squared Error of the position coordinates

$$L(\pi) = \sum_{t}^{T}(P^t - P_r^t)^2. \tag{18}$$

E. Lissajous Trajectory

The controllers are also tested on a Lissajous trajectory. The Lissajous trajectory is not observed by any controller in the training environment, ensuring that the controllers and parameters are not overfitting to any single trajectory. The Lissajous trajectory is a good choice for our Out-Of-Distribution (OOD) testing, as it provides a strong snap impulse error to the controller reference error. Testing the controllers on two complex trajectories, each with its own difficulties, demonstrates the controllers' robustness across various trajectory types.

We formulate the trajectory reference as

$$P_r^t = \begin{bmatrix} R_x\sin(\kappa_x t) \\ R_y\sin(\kappa_y t + \phi_y) \\ A_z\sin(\kappa_z t + \phi_z) \end{bmatrix} \tag{19}$$

with κ_x, κ_y, and κ_z controlling the frequency of oscilations across each axis. No starting position offset is used for the Lissajous trajectory.

F. PID+DOB controller

One baseline controller used to compare the generated model's performance is a PID cascade controller with a Disturbance Observer (DOB), which provides online parameter updates to compensate for model inaccuracies.

PSO-optimised gains (gathered from running the PID+DOB controller in the training environment) for the PID cascade are provided as:

TABLE II: PID Cascade Gains

Controller	P Gain	I Gain	D Gain
Position X	2.48209	N/A	2.02742
Position Y	3.53132	N/A	1.62606
Position Z	7.12605	N/A	1.62871
Orientation	12	0	0
Angular Velocity	4.5	4.5	4.0

The **I** term is not used within the velocity and position controller, with the multiplicative integration value instead replaced directly by the DOB output. The DOB output is based on a plant model of the UAV and updated per-timestep. Fixed gains were used for the orientation and angular velocity reference error to prevent the system from exhibiting aggressive behaviours in deployment.

As a quadcopter is underactuated and only produces collective thrust for positional translations, we convert the required linear accelerations from the velocity PD+DOB into orientations through the formula:

$$\omega_t^x = atan2\left(||V_t'^x||, ||V_t'^z||\right) \tag{20}$$

$$\omega_t^y = -atan2\left(||V_t'^y||, ||V_t'^z||\right) \tag{21}$$

$$\omega_t^z = 0 \tag{22}$$

using small-angle approximation. Here, ω_t^x is the target roll, ω_t^y the pitch target, and ω_t^z the yaw target.

To convert the desired angular velocity into body torque for the fixed frame, we use the following equation, derived and provided by the equations within the simulation:

$$b = IG\omega_t' + \omega' \times (I\omega'). \tag{23}$$

Here, G represents a diagonal matrix of P gains for the conversion from angular velocity into desired body torque (b).

G. LQR controller

Each timestep, the LQR controller receives a state x

$$x = \begin{bmatrix} P_x & P_y & P_z & P'_x & P'_y & P'_z & \phi & \theta & \psi & p \\ q & r & & & & & & & & \end{bmatrix}^\top \in \mathbb{R}^{12}, \tag{24}$$

where $P = [x\ y\ z]^\top$ is the position, $P' = [P'_x\ P'_y\ P'_z]^\top$ the linear velocity, $\eta = [\phi\ \theta\ \psi]^\top$ the roll, pitch, and yaw Euler angles, and $\omega = [p\ q\ r]^\top$ the body angular rates.

The control input vector u defined as

$$u = \begin{bmatrix} T & \tau_x & \tau_y & \tau_z \end{bmatrix}^\top. \tag{25}$$

where T is the total collective thrust and τ_x, τ_y, τ_z are the body torques.

The nonlinear dynamics are linearised into a state-space model around the hover point using A and B:

$$\dot{x} = Ax + Bu, \tag{26}$$

with the A given by

$$A = \begin{bmatrix} 0_{3\times3} & I_3 & 0_{3\times3} & 0_{3\times3} \\ 0_{3\times3} & 0_{3\times3} & \begin{matrix} 0 & g & 0 \\ -g & 0 & 0 \\ 0 & 0 & 0 \end{matrix} & 0_{3\times3} \\ 0_{3\times3} & 0_{3\times3} & 0_{3\times3} & I_3 \\ 0_{3\times3} & 0_{3\times3} & 0_{3\times3} & 0_{3\times3} \end{bmatrix}, \tag{27}$$

and B provided as

$$B = \begin{bmatrix} & 0_{3\times4} & \\ 0 & 0 & 0 & 0 \\ 0 & 0 & 0 & 0 \\ \frac{1}{m} & 0 & 0 & 0 \\ & 0_{3\times4} & \\ 0 & \frac{1}{I_x} & 0 & 0 \\ 0 & 0 & \frac{1}{I_y} & 0 \\ 0 & 0 & 0 & \frac{1}{I_z} \end{bmatrix}, \tag{28}$$

.

TABLE III: LQR Gains

ID	XY Gain	Z Gain
Q_pos	20.418293	19.739102
Q_vel	1.104827	0.982716
Q_ang	5.291844	0.918472
Q_rate	0.108472	0.094821
R_thrust	N/A	0.091847
R_torque	1.048271	0.962819

We formulate the state ~~weighting~~ matrix Q as

$$Q = \mathrm{diag}\big(Q_{\text{pos},xyz}\,\text{pos},xy,z,\ Q_{\text{vel},xyz}\,\text{vel},xy,z,\ Q_{\text{ang},xyz}\,\text{ang},xy,z,\ Q_{\text{rate},xyz}\,\text{rate},xy,z\big), \tag{29}$$

and the ~~control~~ effort matrix R as

$$R = \mathrm{diag}\big(R_{\text{thrust}},\ R_{\text{torque},xyz}\,\text{torque},xy,z\big). \tag{30}$$

The optimal feedback gain is obtained from the continuous-time Algebraic Riccati Equation (ARE)

$$A^\top P + PA - PBR^{-1}B^\top P + Q = 0, \tag{31}$$

whose solution $P \in \mathbb{R}^{12\times12}$ yields the optimal gain

$$K = R^{-1}B^\top P \in \mathbb{R}^{4\times12}. \tag{32}$$

The ARE is solved iteratively by integrating

$$\dot{P} = A^\top P + PA - PBR^{-1}B^\top P + Q. \tag{33}$$

~~To implement the controller, let~~

~~$$x_d = \begin{bmatrix} p_d^\top & v_d^\top & \eta_d^\top & \omega_d^\top \end{bmatrix}^\top$$~~

~~denote the desired state. The state error is defined as~~

~~$$e = \begin{bmatrix} p - p_d \\ v - v_d \\ \eta - \eta_d \\ \omega - \omega_d \end{bmatrix}.$$~~

~~The control input is computed as~~

~~$$u = u_{\text{eq}} - Ke,$$~~

~~with the hover equilibrium input~~

~~$$u_{\text{eq}} = \begin{bmatrix} mg \\ 0 \\ 0 \\ 0 \end{bmatrix}.$$~~

~~The state~~ The state and control gains Q and R are obtained by running the controller in the training environment and estimating via PSO. We perform this tuning the same across all controllers. The gains for the LQR controller are provided in Table **??**

IV. Training Results

Training results for the generated controller are provided in Figure **??**. ~~The final SSE~~ In Figure **??**, we can see close agreement between the control system and provided trajectory. The final MSE for the generated controller in the training environment was ~~62.433~~0.0062433m^2 (after fine-tuning with PSO), with the ~~inital controller achieveing~~ initial controller achieving an MSE of ~~1652.80~~0.165280m^2. The generated controller demonstrates accurate path following for the lemniscate trajectory. Qualitatively, the UAV's motion appears smooth and closely matches the desired trajectory, with no apparent issues. This outcome is comparable to advanced controllers in the literature that follow lemniscate trajectories with minimal error.

V. Generated Controller

The generated controller itself closely resembles the initial input PID controller we used. Interestingly, this controller does not contain a disturbance observer. The differences between the controller and a standard UAV controller are as follows: velocity and orientation smoothing; dynamic gains based on the smoothed velocity magnitude; clamping; and anti-windup. It is interesting to see that addition of these small changes create improvements in comparison to a more complex control system implementation (i.e. LQR). For further investigation of the generated control system, it is recommended to view the control system implementation within the associated GitHub repository [**?**].

Fig. 2: **Training results:** Generated control system output in the training environment vs baseline trajectory. The trajectory to be followed is shown as a dotted line. Also indicated here is the large positional offset the controller begins with, allowing for estimation of controller performance to both large and small reference discrepancies in a single simulation run.

A. *Software-in-the-loop (SITL) testing*

While it is possible to skip a custom simulator and use Gazebo directly to create controllers, it is not recommended. If a controller is 'built' while using Gazebo as a training environment in an attempt for direct deployment (Gazebo to real world), a large risk of overfitting remains. We use Gazebo here as the second environment to check for overfitting and confirm the control systems can interpolate information within new, unseen environments.

As the generated controller produced acceptable results in the training environment, we prepared the algorithm for real-world deployment by transitioning it into a ROS 2 node that interfaces with PX4. PX4 enables SITL testing before deployment with high-fidelity simulations that integrate seamlessly into PX4 firmware. The SITL simulations offer a form of OOD testing and are higher quality and offer more insight into actual UAV performance than our training environment [**?**], [**?**].

The ROS2 node was integrated into PX4 Autopilot using the Micro-XRCE-DDS bridge. PX4 utilises a publisher/subscriber design pattern to exchange information between the onboard flight controller and an offboard controller. This integration allows us to treat the generated controller as a part of the PX4 firmware, benefiting from low-latency communication and access to internal state estimations. The generated controller, as a ROS 2 node, required some minor implementation changes before it functioned as intended. PX4 requires that the controller output is both normalised relative to the motor output and in a NED world frame. The generated controller, as designed, outputs absolute torque and thrust values (N) in a FLU world frame. We send the thrust and torque commands to PX4 at a rate of 8ms, with the controller receiving sensor updates at the same rate.

A diagram illustrating the interaction between the generated controller and PX4 via PX4 topics is shown in Figure **??**.

TABLE IV: Per-lap Performance Metrics Comparison SITL

Controller	MSE	Std. dev	Best MSE
Lemniscate (SITL)			
Generated Controller	**0.0304**m^2	0.0031m^2	**0.0245**m^2
PID+DOB	0.0418m^2	**0.0012**m^2	0.0393m^2
LQR	0.0533m^2	0.0143m^2	0.0744m^2
Lissajous (SITL)			
Generated Controller	**0.0084**m^2	**0.0006**m^2	**0.0071**m^2
PID+DOB	0.0107m^2	0.0008m^2	0.0088m^2
LQR	0.0116m^2	0.0017m^2	0.0090m^2

Table **??** quantitatively summarises the results of 10 laps in the SITL testing environment for both the lemniscate and Lissajous trajectories.

TABLE V: Per-lap Performance Metrics Comparison SITL

Controller	Rise time	Settling time	s error
Generated controller	1.296s	3.832s	0.003m
PID+DOB	**0.776**s	**2.504**s	**0.001**m
LQR	1.120s	2.792s	0.003m

Additional SITL tests were performed to confirm the UAV control system's response against more classical metrics, summarised in Table **??**. Note here that s error refers to the steady state error of the UAV.

On the lemniscate trajectory, the generated control system ~~offered~~ achieved a mean performance increase of 27.27% ~~compared to~~ over the best-performing hand-made controller (PID+DOB). The worst lap of the generated control system outperformed the best lap of the PID+DOB control system. The reduced variance and standard deviation within laps of the PID+DOB control system are likely due to the DOB controller reaching its disturbance-estimation limits in the presence of model inaccuracies. For the generated control system, no disturbance observer or online model estimation is available, which contributes to ~~the increased variation per lap~~increased lap-to-lap variation.

SITL results are displayed visually in Figure **??**. In Figure **??**, we can see that the generated controller offered substantial improvement across most axis within all tasks. In some areas, specifically P_z error within the Lissajous task, we can see large inital error within the control system. Postulations for this are that the sliding window used by the control system did not correctly handle a large inital input disturabance by the Lissajous trajectory.

VI. Deployment and Real World Results

Results are gathered using a UAV inside the Autonomous Systems lab at Loughborough University. We conducted 10 flight experiments for each controller, across both Lemniscate and Lissajous trajectories. During deployment, there was little variability within the results, and no failed flights. We took

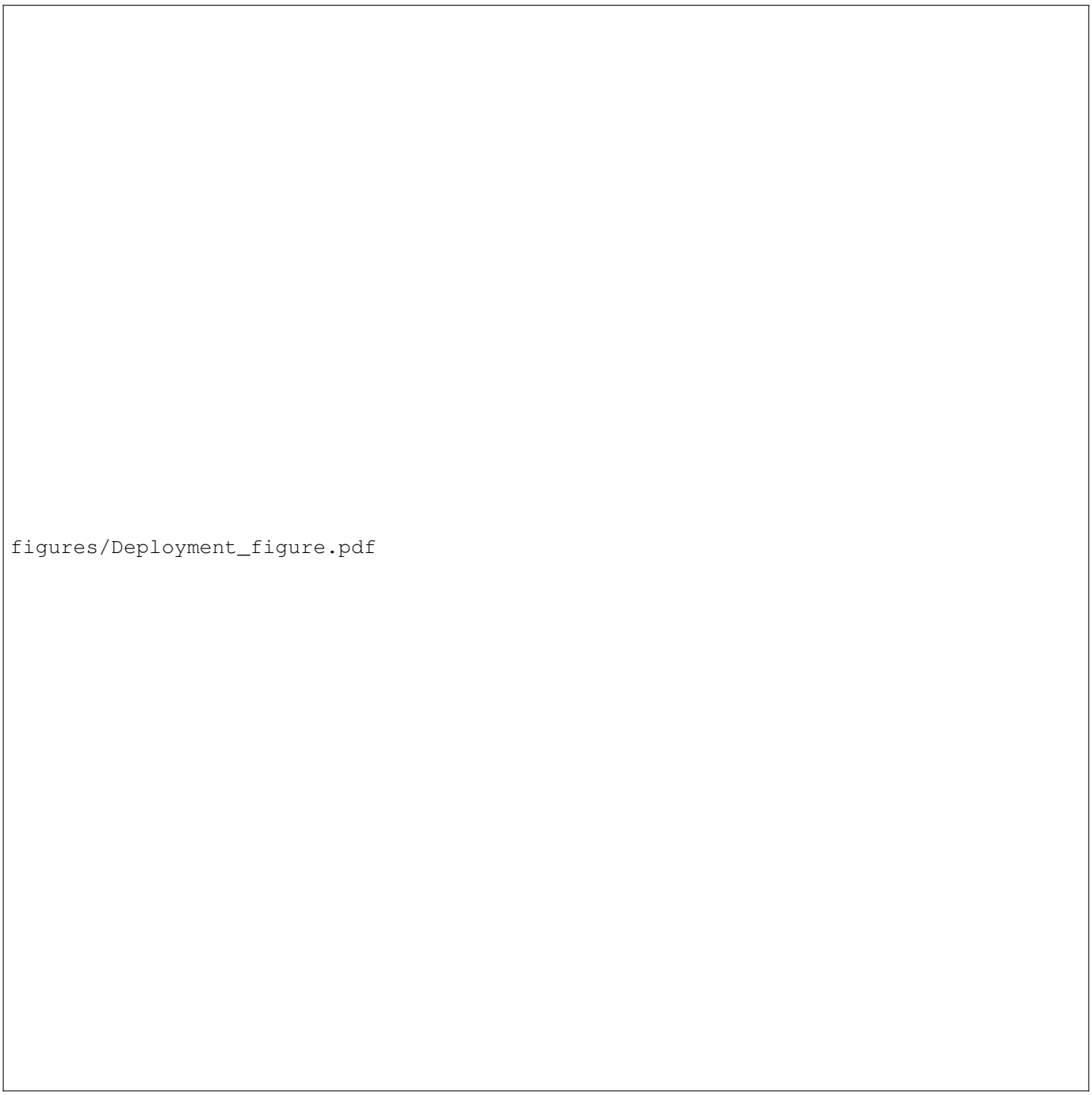

Fig. 3: Real-world deployment of the generated control system onto a UAV with a motion capture system. The motion capture system sends precise position and orientation information to the companion computer~~through a TCP connection in an ENU coordinate frame~~. The companion computer ~~converts the ENU frame into a NED frame and publishes it to the PX4 board. The PX4 board~~ sends ~~vehicle odometry gathered from an Extended Kalman Filter (EKF) back to the companion computer, which subsequently sends~~ body-torque and collective thrust commands to the ~~microprocessor~~PX4 microcontroller. The ~~microprocessor~~ microcontroller performs control allocation to convert the normalised thrust commands into PWM commands and interfaces them to the motors.~~The motors produce thrust, which alters the forces acting on the UAV, thereby changing its position and orientation.~~

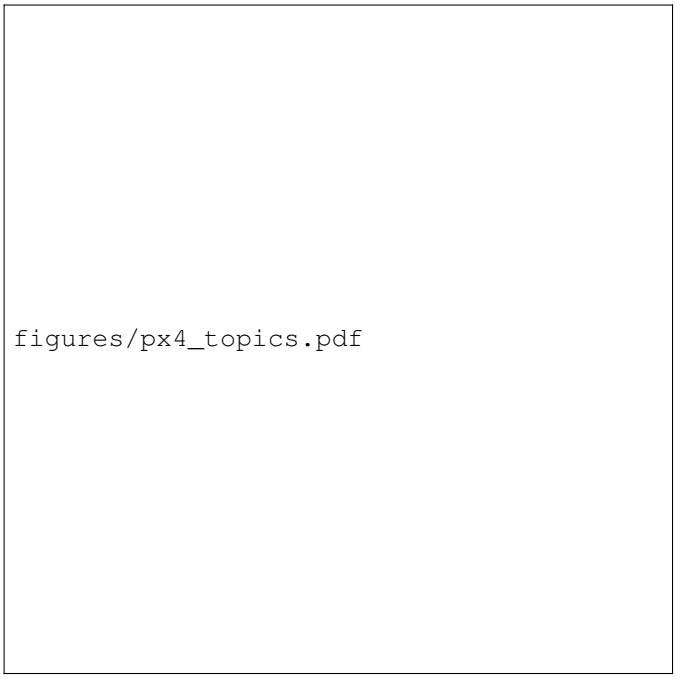

Fig. 4: **PX4-ROS 2 interation:** Interaction between PX4 and the ROS2 nodes via a publisher/subscriber design pattern.

safety measures to ensure the control systems did not cause damage to the environment: a designated experiment area that the operator cannot enter during flight, the UAVs are suspended via a pulley system such that they cannot fall from height, a kill switch on the UAVs to immediately cut power, and finally a fallback to PX4 in-built flight control system if the offboard control system fails to send a heartbeat for 100ms.

The UAV is built using a Holybro Pixhawk 6X, which houses and runs the PX4 firmware. A USB connecting the companion computer and flight controller are plugged into the Holybro Pixhawk 6X. For real-world deployment, instead of using the position and orientation information provided by the PX4 IMU, we use a VICON motion tracking system, which overrides the PX4-provided estimates. The motion tracking system provides more accurate estimates of the UAV's position, velocity, and orientation. Figure **??** describes our deployment setup in a visual format, whereby each component is shown with relative outputs and inputs.

The results of the experiments for the real-world experiments are also visualised in Figure **??**.

TABLE VI: Per-lap Performance Metrics Comparison Real world

Controller	MSE	Std. dev	Best MSE
Lemniscate (REAL WORLD)			
Generated Controller	**0.0098**m^2	**0.0010**m^2	**0.0090**m^2
PID+DOB	0.0329m^2	0.0125m^2	0.0187m^2
LQR	0.0261m^2	0.0028m^2	0.0201m^2
Lissajous (REAL WOLRD)			
Generated Controller	**0.0084**m^2	**0.0006**m^2	**0.0071**m^2
PID+DOB	0.0116m^2	0.0008m^2	0.0088m^2
LQR	0.0116m^2	0.0017m^2	0.0090m^2

~~A results Table for the real-world results is~~ Results are provided in Table **??**. Within the results, the average is taken over 10 laps of the trajectory. 'MSE' refers to the MSE of all laps, and 'Best MSE' is the lap with the lowest MSE. The generated controller yielded strong results in the real world. An MSE of 0.0098 m^2 precision within the lemniscate trajectory highlights the strengths of our methodology, whilst also showcasing areas for improvement. We specifically highlight the area for improvement in our results, namely, the direct deployment and iteration in the real world.

The generated controller exhibited greater robustness than the PID+DOB. All runs were performed across two charge cycles of a lithium-ion battery, with each run using approximately 20% of the battery charge. We observe sensitivity to battery charge across runs in the PID+DOB controller. The achieved Z-axis component is reduced as the battery charge decreases. Unlike the PID+DOB controller, the generated control system shows no sensitivity to the charge, with the achieved accuracy remaining consistent throughout the experiments.

The achieved accuracy is higher for the generated control system than for the baseline controller. Across the X and Y axes. The generated control system achieved close agreement with the target tracking across the Z-component throughout all experiments.

It is possible that both control systems can achieve better performance through real-world specific tuning. It is important to note that these results are obtained without any tuning in either SITL testing or the real world. The entire process is automatic: the gains for the control systems are determined using PSO within the training simulator.

VII. Conclusion

In conclusion, we have designed and tested an LLM-synthesised control system using two simulators. The simulators showed that the generated control system is reliable for unmanned flight.

After testing the control system in the real world, we provide proof that generated code can be used in a Reinforcement Learning-esque fashion to create functional real-world code.

Because we used a training environment, the generated controllers are subject to the same limitations as reinforcement learning, such as overfitting to the training environment (known as the sim-to-real gap). We base this conclusion on a 3x reduction in performance from the training environment to the real world. Also notable is the lack of online parameter estimation for the generated control systems. The cause is primarily our methodology. No online parameter estimation is required, as PSO already optimises the model towards our known model parameters during the simulation.

The choice of our task, unmanned flight, reflects the growth and capabilities of LLMs to synthesise high-quality code across many queries.

This work opens the door to the application of agentic AI in engineering design and to the creation of many different control systems for the real world. Primarily, the following steps in this work are the creation of certified control systems, which can each be tested in the real world without the need for an intermediate testing environment.

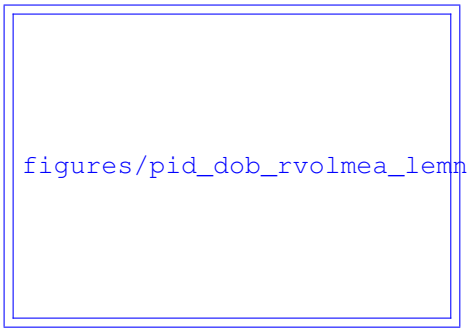

(a) P_x error, Lemniscate (SITL)

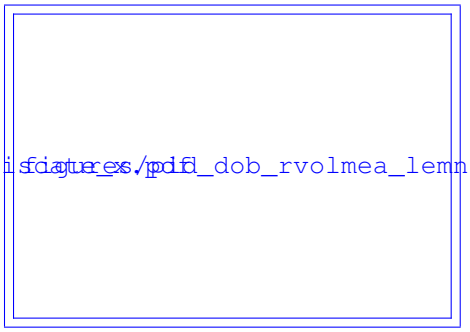

(b) P_y error, Lemniscate (SITL)

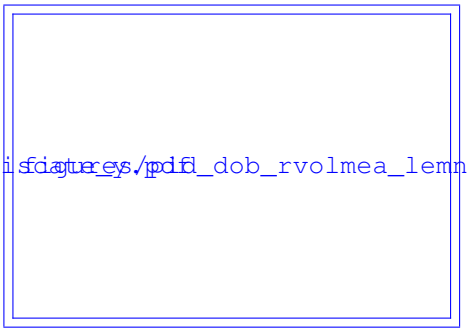

(c) P_z error, Lemniscate (SITL)

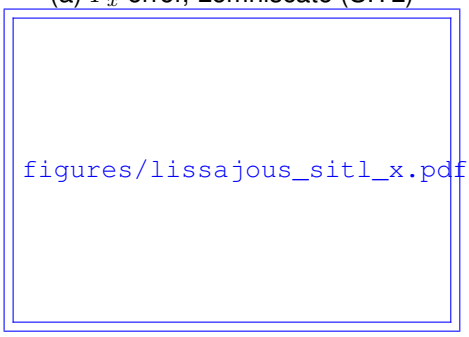

(d) P_x error, Lissajous (SITL)

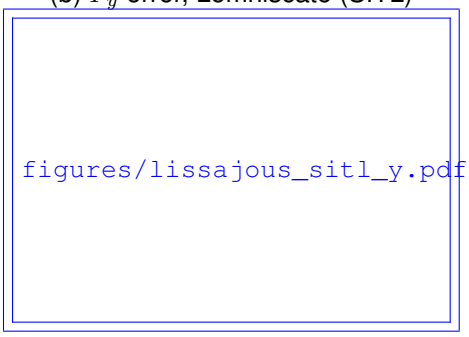

(e) P_y error, Lissajous (SITL)

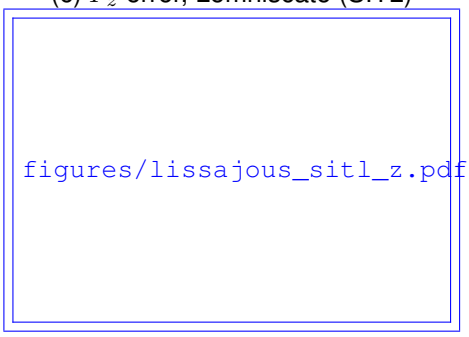

(f) P_z error, Lissajous (SITL)

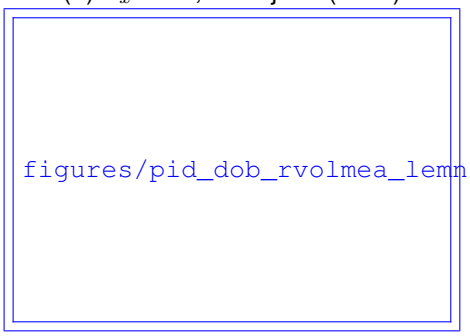

(g) P_x error, Lemniscate (Real-world)

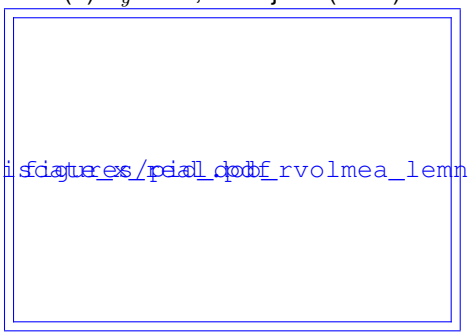

(h) P_y error, Lemniscate (Real-world)

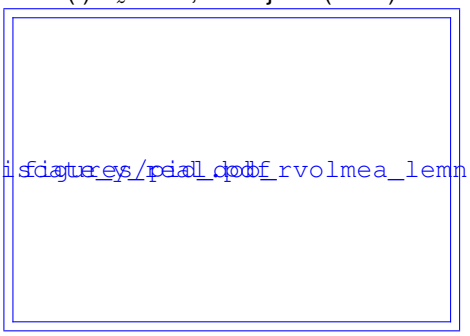

(i) P_z error, Lemniscate (Real-world)

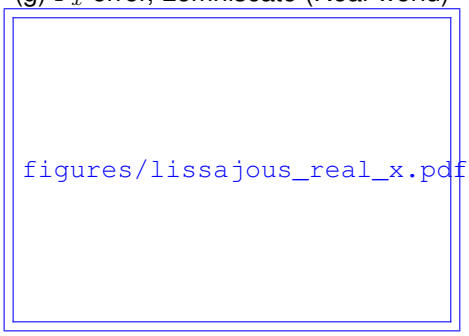

(j) P_x error, Lissajous (Real-world)

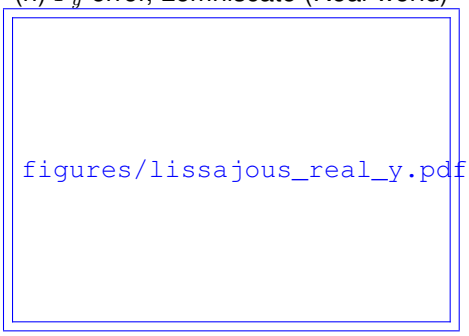

(k) P_y error, Lissajous (Real-world)

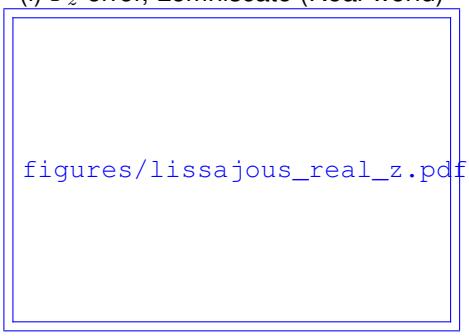

(l) P_z error, Lissajous (Real-world)

Fig. 5: ~~**Results:**~~ **Results:** Comparison of SITL and real-world tracking errors for the ~~lemniscate~~ Lemniscate and Lissajous trajectories. ~~The label~~ RVOLMEA ~~is used to identify~~ denotes the generated ~~control system~~controller. ~~Variation between SITL and real-world results is expected, given the change in environments. Consistent with the existing literature, the SITL results are closer to real-world results than those from the training environment. The figures~~ Subfigures (a)–(l) show ~~the reference~~ axis-wise tracking error over time for the best lap ~~of any given controller (the~~ lowest MSE~~lap~~).

For future works, there are two main directions of focus. Firstly, it will be interesting to see this work applied to general purpose robotics-based tasks. The work here is applied to a control system, though the task itself can be anything that is measured via an objective function. Secondly, the removal of PSO for other techniques is a viable place for exploration. It will be interesting to see if evolution in the surrogate optimisation function over time, hand-in-hand with

the primary candidate function, results in general improvement of the algorithm.

Creating a methodology for unmanned flight is difficult. Simulated training environments are almost always required because poor control systems can lead to catastrophic failure in the real world. It would be interesting to apply this methodology directly to the real world, using online parameter estimation rather than PSO. This way, the limitations identified in this paper (overfitting and lack of generalisation) can be mitigated through real-world scoring and iteration. These control systems would need to be implemented on an unmanned vehicle, such as a TurtleBot, that is not in any intrinsic danger, so that faulty control systems can be easily discarded without damaging the machine executing them. A link for viewing the ~~implementation of all controllers with the lemniscate trajectory is provided~~ https://github.com/jynxmagic/Px4-offboard-controllers-thrust-and-torque~~here. The generated control system can be found under the function 'rvolmeaControl'~~ code used to generate the control system and deploy the control system to the UAV is provided in the references [**?**].